

OccFusion: A Straightforward and Effective Multi-Sensor Fusion Framework for 3D Occupancy Prediction

Zhenxing Ming, Julie Stephany Berrio, Mao Shan, and Stewart Worrall

Abstract—This paper introduces OccFusion, a straightforward and efficient sensor fusion framework for predicting 3D occupancy. A comprehensive understanding of 3D scenes is crucial in autonomous driving, and recent models for 3D semantic occupancy prediction have successfully addressed the challenge of describing real-world objects with varied shapes and classes. However, existing methods for 3D occupancy prediction heavily rely on surround-view camera images, making them susceptible to changes in lighting and weather conditions. By integrating features from additional sensors, such as lidar and surround view radars, our framework enhances the accuracy and robustness of occupancy prediction, resulting in top-tier performance on the nuScenes benchmark. Furthermore, extensive experiments conducted on the nuScenes dataset, including challenging night and rainy scenarios, confirm the superior performance of our sensor fusion strategy across various perception ranges. The code for this framework will be made available at <https://github.com/DanielMing123/OCCFusion>.

Index Terms—autonomous driving, 3D semantic occupancy prediction, environment perception

I. INTRODUCTION

UNDERstanding and modelling the three-dimensional (3D) world of surrounding scenes is essential for autonomous driving to prevent collisions and facilitate local planning. As technology advances, the introduction of 3D occupancy representation has successfully addressed the limitations of traditional 3D object detection networks, particularly for detecting irregular objects and space-occupied status prediction. This advancement further enhances the capability of smart vehicles to model the 3D world. However, the currently proposed 3D occupancy prediction models [1]–[6], [6]–[14], primarily focus on vision-based approaches (Figure 1, upper). While surround-view cameras are cost-effective, their perception capabilities are highly susceptible to various weather conditions, such as sunny, rainy, foggy, and different illumination conditions, like daytime and nighttime. These factors cause the model to perform inconsistently in these scenarios, thereby posing potential safety risks.

Besides the surround-view cameras, modern smart vehicles are also equipped with advanced lidar and surround-view millimetre wave radars. Lidar excels at capturing the geometric shape of objects and accurately measuring depth. Moreover, it is resistant to changes in illumination and performs reliably

This work has been supported by the Australian Centre for Robotics (ACFR). The authors are with the ACFR at the University of Sydney (NSW, Australia). E-mails: zmin2675@uni.sydney.edu.au, [j.berrio, m.shan, e.nebot, s.worrall}@acfr.usyd.edu.au](mailto:{j.berrio, m.shan, e.nebot, s.worrall}@acfr.usyd.edu.au)

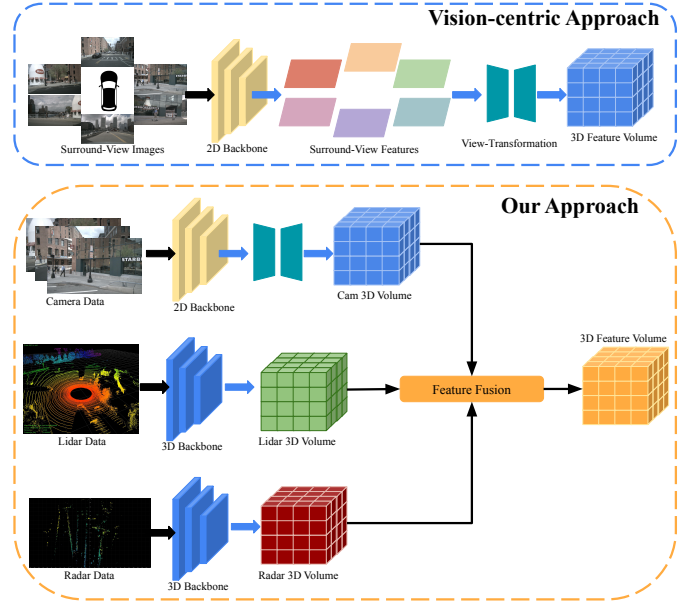


Fig. 1: The figure above demonstrates the pipeline of two approaches: The purely vision-centric approach (top) and the multi-sensor fusion approach (bottom). We conduct 3D semantic occupancy prediction by doing feature fusion with respect to three modality feature volumes.

under various weather conditions, except for heavy rain and fog. In contrast, surround-view millimetre wave radars are cost-effective and exceptionally robust against weather conditions and changes in illumination. However, they yield only sparse features, which are often noisy. Each sensor possesses its advantages and disadvantages. We argue that combining information from all three sensors (Figure 1, bottom) can empower smart vehicles’ 3D occupancy prediction model to achieve superior comprehension and modelling of the 3D world. Additionally, this integration improves the system’s robustness in the face of varying lighting and weather conditions.

To predict 3D occupancy accurately and efficiently, we propose a framework called OccFusion. This framework merged features from surround-view cameras, surround radars, and 360 degree lidar through proposed dynamic fusion 3D/2D modules. There are three sensor fusion strategies, namely, Camera + Radar, Camera + Lidar, and Camera + Lidar + Radar. To evaluate the effectiveness of our sensor fusion strategies, we conduct experiments on the nuScenes dataset [15],

utilizing ground truth labels provided by the SurroundOcc [7] and Occ3D [6]. Additionally, we manually select rainy and nighttime scenarios from the nuScenes validation set to create two challenging subsets and examine the performance of different sensor fusion strategies in these scenarios. Finally, we test how the performance of different sensor fusion strategies varies across different perception ranges under different scenarios.

The main contributions of this paper are summarized below.

- A multi-sensor fusion framework is proposed to integrate camera, lidar, and radar information for the task of 3D semantic occupancy prediction.
- We compared our approach with other state-of-the-art (SOTA) algorithms in the 3D semantic occupancy prediction task to prove the advantages of multi-sensor fusion.
- We conducted thorough ablation studies to assess the performance gains achieved by different sensor combinations under challenging lighting and weather conditions, such as night and rainy scenarios.
- We conducted a comprehensive study to analyze the influence of perception range factors on the performance of our framework in 3D semantic occupancy prediction tasks, considering various sensor combinations and challenging scenarios.

The remainder of this paper is structured as follows: Section II provides an overview of related research and identifies the key differences between this study and previous publications. Section III outlines the general framework of OccFusion and offers a detailed explanation of the implementation of each module. Section IV presents the findings of our experiments. Finally, Section V provides the conclusion of our work.

II. RELATED WORK

A. Camera-only environment perception

In recent years, surround-view camera-based environment perception algorithms have received significant attention in the autonomous driving domain due to their cost-effectiveness and versatility. The BEV feature-based algorithms [2]–[4], [16]–[19] successfully merged all surround-view camera information to conduct 3D object detection tasks. By lifting the BEV feature into 3D feature volume, algorithms [2], [10] are capable of doing 3D semantic occupancy tasks. There are two main approaches to view transformation in these algorithms: the classic Lift-Splat-Shoot (LSS) approach and the transformer-based approach. The LSS-based approach [12], [20] relies on depth estimation to generate a pseudo-3D point cloud, followed by voxel-pooling to create the final 3D feature volume. On the other hand, the transformer-based approach [5]–[9], [11], [13] uses sampling points to aggregate visual features from feature maps and places these features directly at specific 3D positions in the world to form the final 3D feature volume. Both approaches either explicitly estimate the depth or implicitly encode depth information in visual features. Nonetheless, it is well-known that monocular cameras are inadequate for accurate depth estimation. While they can capture the relative depth position of an object, they cannot provide precise depth information. Hence, a more reliable

reference for depth information is required. This could involve incorporating lidar information into the model to enhance depth estimation or using lidar information to supervise depth estimation, as in the BEVDet series approaches.

B. Lidar-only environment perception

Lidar-based algorithms [21]–[31] for environment perception have shown promising performance in various perception tasks. Leveraging its capability for accurate depth estimation, lidar excels in capturing the geometric shape and 3D location of objects. By converting the 3D point cloud into Euclidean feature spaces, such as 3D voxel grids [32] or feature pillars [33], lidar-based methods can achieve highly precise 3D object detection results. In recent years, researchers have extended lidar’s 3D point cloud features into 3D semantic occupancy prediction tasks [34], [35]. However, the density of the lidar-generated 3D point cloud strongly influences the final perception performance of the model, and its lack of semantic information results in inaccurate object class recognition. Hence, the auxiliary information is needed to provide comprehensive semantic information guidance, which leads to our work fusing the lidar data with camera data to enhance the performance of 3D semantic occupancy prediction.

C. Camera-Lidar fusion environment perception

Due to the inherent advantages and disadvantages of individual sensors, recent research has focused on sensor fusion techniques [36]–[41] to overcome these limitations and enhance the overall environment perception capability of the models. The representative BEVFusion [42], [43] algorithms fuse lidar and surround-view cameras by encoding the features of each modality into BEV features and performing feature fusion. This approach addresses the reflection issues encountered by lidar in rainy and foggy scenarios, which often result in false detections and missed detections. It also resolves the poor depth estimation problem of monocular cameras, enabling the model to generate relatively accurate detection results at longer distances. The SparseFusion [44] further refines the inner structure of the feature fusion module, greatly improving the model’s inference speed. However, it is regrettable that currently there are no camera-lidar fusion algorithms specifically designed for the 3D semantic occupancy prediction task; the majority of existing algorithms primarily serve for 3D object detection. Therefore, there is a compelling need for extensive research on camera-lidar fusion techniques for 3D semantic occupancy prediction.

D. Camera-Radar fusion environment perception

Various studies [45]–[47] have been conducted on the fusion of cameras and radar for environmental perception due to radar’s cost-effectiveness and ability to detect distant objects. For instance, the work carried out in [48] demonstrates that information about velocity obtained from radar sensors can enhance detection performance. Additionally, a study by [49] suggests that integrating radar features with visual features can result in a performance gain of approximately 12% under the

nuScene Detection Score (NDS) metric. Furthermore, another study in [50] found that radar sensor readings exhibit robustness in noisy conditions, and integrating radar information can improve model performance in challenging scenarios. Though various algorithms have been developed to achieve camera-radar fusion, the majority of these algorithms focus on 3D object detection, object tracking, and object future trajectory prediction tasks. There is currently no camera-radar fusion algorithm available specifically for 3D semantic occupancy prediction tasks. Moreover, the task of 3D semantic occupancy prediction requires dense features, whereas radar provides sparse features. Consequently, it is both intriguing and valuable to investigate the impact on model performance when merging these sparse radar features with camera and lidar data. To the best of our knowledge, our study is the first to examine the influence of fused radar information on a 3D semantic occupancy prediction task.

E. Camera-Lidar-Radar fusion environment perception

Due to the complementary property of multi-sensor fusion, people in this domain also investigate the camera-lidar-radar fusion strategy and its performance in environment perception. In CLR-BNN [51], the authors employ a Bayesian neural network for camera-lidar-radar sensor fusion, yielding improved 2D multi-object detection results in terms of mAP. In Futr3D [52], the sensor fusion is further explored through the incorporation of transformers, using sparse 3D points as queries to aggregate features from the three sensors for the 3D object detection task, the query-form significantly improved feature interactions and aggregation efficiency across three sensors. In SimpleBEV [53], authors process data from all three sensors into Bird’s Eye View (BEV) features, fusing these features based on three BEV representations to perform the 3D object detection task; in their research, they found radar data provide a substantial boost to performance. Previous research has extensively examined the characteristics of three sensor fusion methods for environmental perception. However, these works have primarily concentrated on 2D or 3D multi-object detection tasks, neglecting investigations into the 3D semantic occupancy prediction task. Therefore, there is a need to investigate the performance of the camera-lidar-radar sensor fusion strategy in the context of 3D semantic occupancy prediction tasks.

III. OCCFUSION

A. Problem Statement

This paper aims to generate a dense 3D semantic occupancy grid of the surrounding scene by integrating information from surround-view cameras $Cam = \{Cam^1, Cam^2, \dots, Cam^N\}$, surround-view radars $Rad = \{Rad^1, Rad^2, \dots, Rad^N\}$, and lidar Lid . Thus, the problem can be formulated as:

$$Occ = F(Cam^1, \dots, Cam^N, Rad^1, \dots, Rad^N, Lid) \quad (1)$$

where F represents the fusion framework that integrates multi-sensor information for 3D occupancy prediction. The final 3D occupancy prediction result is represented by $Occ \in$

$R^{X \times Y \times Z}$, where each grid is assigned a semantic property and has a value ranging from 0 to 16. In our case, a class value of 0 corresponds to an empty grid.

B. Overall Architecture

Figure 2 exhibits the overall architecture of our proposed framework. Initially, given surround-view images, dense 3D point clouds P^{Dense} from lidar and sparse 3D point clouds P^{Sparse} from surround-view radars, we apply a 2D backbone (e.g. ResNet101-DCN) to extract total L scale features $M = \left\{ \left\{ M_n^l \right\}_{n=1}^N \in R^{C_l \times H_l \times W_l} \right\}_{l=1}^L$ from images, followed by view transformation to obtain the global BEV feature $F_{global}^{Cam,l} \in R^{C_l \times X_l \times Y_l}$ and local 3D feature volume $F_{local}^{Cam,l} \in R^{C_l \times X_l \times Y_l \times Z_l}$ at each scale. Meanwhile, a 3D backbone (e.g. VoxelNet) is also applied to dense and sparse 3D point clouds to generate multi-scale global BEV features $F_{global}^{Rad,l} \in R^{C_l \times X_l \times Y_l}$, $F_{global}^{Lid,l} \in R^{C_l \times X_l \times Y_l}$ and local 3D feature volumes $F_{local}^{Rad,l} \in R^{C_l \times X_l \times Y_l \times Z_l}$, $F_{local}^{Lid,l} \in R^{C_l \times X_l \times Y_l \times Z_l}$, respectively. Following that, the $F_{global}^{Cam,l}$, $F_{global}^{Rad,l}$ and $F_{global}^{Lid,l}$ at each level are fed into the dynamic fusion 2D module to obtain the merged global BEV feature $F_{global}^{Merged,l}$. Simultaneously, the $F_{local}^{Cam,l}$, $F_{local}^{Rad,l}$ and $F_{local}^{Lid,l}$ at each level are also fed into the dynamic fusion 3D module to obtain the merged local 3D feature volume $F_{local}^{Merged,l}$. Subsequently, the global-local attention fusion module proposed in [14] is used at each level to further merge $F_{local}^{Merged,l}$ and $F_{global}^{Merged,l}$, resulting in the final 3D volume at each level. Moreover, a skip-connection structure is implemented between each level to refine the features in a coarse-to-fine manner, and multi-scale supervision is applied to improve the model’s performance.

C. Surround-View Images Feature Extraction

Given surround-view images, we initially employ ResNet101-DCN [54] as our 2D backbone and feature pyramid network (FPN) [55] as the neck to extract multi-scale feature maps. The resulting feature maps have resolutions that are $\frac{1}{8}$, $\frac{1}{16}$, and $\frac{1}{32}$ of the input image resolution, respectively. Subsequently, a view transformation is leveraged, yielding multi-scale global BEV features and local 3D feature volumes. The global and local features with smaller resolutions contain valuable semantic information, aiding the model in predicting the semantic class of each voxel grid. Conversely, those features with larger resolutions provide rich spatial information, enabling the model to determine whether the current voxel grid is occupied or unoccupied.

D. Lidar Dense 3D Point Cloud Feature Extraction

In this paper, we adopt VoxelNet [32] as our 3D backbone for feature extraction of the 3D point cloud. We begin by voxelizing the 3D point cloud to generate the voxel grid and its associated coordinates. For each voxel grid that contains 3D points, we randomly select 35 points. Each point, denoted as p_i^{Lid} , includes an initial feature vector $p_i^{Lid} = [x_i, y_i, z_i, \gamma_i]$ that represents the point’s 3D position and reflectance rate.

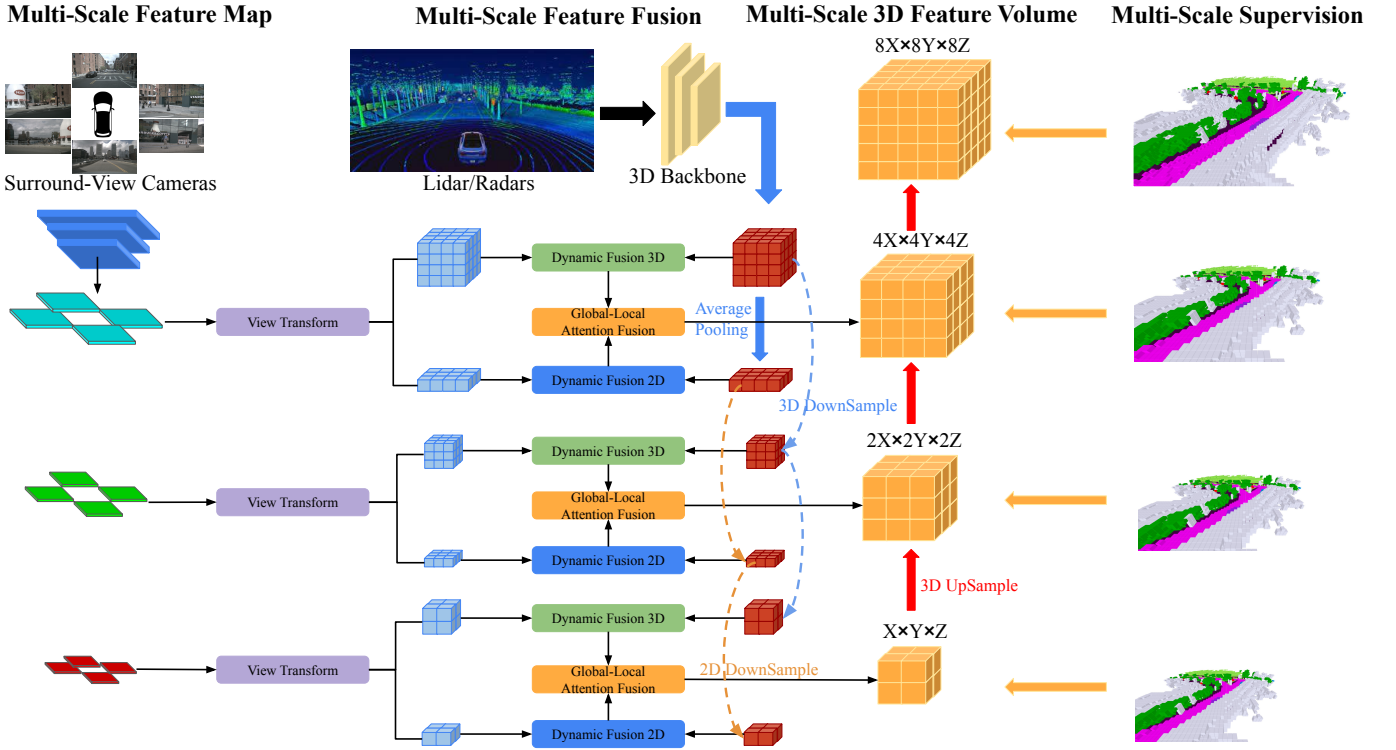


Fig. 2: **Overall architecture of OccFusion.** Firstly, the surround-view images were inputted into the 2D backbone to extract multiple-scale features. Subsequently, a view transformation is conducted at each scale to obtain the global BEV feature and the local 3D feature volume at each level. The 3D point cloud generated by the lidar and surround-view radars is also inputted into the 3D backbone to generate multi-scale local 3D feature volumes and global BEV features. The dynamic fusion 3D/2D modules at each level fuse features from the cameras and lidar/radar. Following this, the merged global BEV feature and local 3D feature volume at each level are fed into the global-local attention fusion to generate the final 3D volume at each scale. Finally, the 3D volume at each level is upsampled, and the skip connection is performed while adopting a multi-scale supervision mechanism.

Subsequently, we calculate the centre position of these 3D points and augment each point with a relative offset with respect to the centre position. This augmentation results in a new feature vector $p_i^{Lid} = [x_i, y_i, z_i, \gamma_i, x_i - \bar{x}, y_i - \bar{y}, z_i - \bar{z}]$. Following this, only the voxel grid with 3D points is input to the 3D backbone to refine the features further, producing the final local 3D feature volume. Additionally, for the global BEV feature, we employ average pooling along the Z-axis of the local 3D feature volume to obtain the flattened global BEV feature. The 3D backbone outputs the highest resolution of the global and local features, while the lower resolution features are obtained through 3D/2D downsampling operations.

E. Radar Sparse 3D Point Cloud Feature Extraction

The Radar 3D point contains richer information compared to the Lidar 3D point. Each Radar 3D point has an initial feature vector $p_i^{Rad} = [x_i, y_i, z_i, V_{xi}, V_{yi}]$, where V_{xi} denote the velocity along the X-axis, and V_{yi} denote the velocity along the Y-axis. Similar to the way used to process the Lidar point cloud, we begin with voxelizing the Radar 3D point cloud and obtain the voxel grids and their associate coordinates. For the voxel grid with points, we calculate the mean value among the 3D points and augment each point with a relative offset with respect to the mean value. This augmentation results in a new feature vector $p_i^{Rad} = [x_i, y_i, z_i, V_{xi}, V_{yi}, x_i - \bar{x}, y_i - \bar{y}, z_i -$

$\bar{z}, V_{xi} - \bar{V}_x, V_{yi} - \bar{V}_y]$. We subsequently input the non-empty voxel grid into the 3D backbone to obtain the local 3D feature volume and then apply average pooling to obtain the global BEV feature.

F. Dynamic Fusion 3D/2D

Drawing inspiration from BEVFusion [42], [43] and SENet [56], this research merges two BEV features and two 3D feature volumes by concatenating their feature channels. Subsequently, a Conv3D/2D layer is applied to reduce the feature channel dimension, facilitating the merging of valuable features from diverse modalities while filtering out noisy features. This process is followed by a 3D/2D SENet block, where the merged features are inputted into the squeeze module (SENet Block 3D/2D Upper) to determine the importance of each feature channel. The excitation module (SENet Block 3D/2D bottom) then implements an excitation procedure by multiplying the merged features with the squeeze feature, enabling critical features to dominate. Details of the Dynamic Fusion 3D module can be found in the upper section of Figure 3, while specifics of the Dynamic Fusion 2D module are depicted in the bottom section of Figure 3.

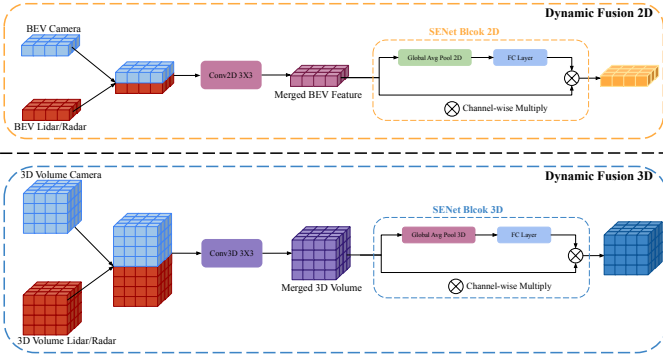


Fig. 3: Dynamic Fusion 3D/2D Modules. The upper diagram exhibits the process details of the dynamic fusion 2D module, and the bottom diagram shows the process details of the dynamic fusion 3D module.

IV. EXPERIMENTAL RESULT

A. Implementation Details

The OccFusion utilizes ResNet101-DCN [57], [58] as the 2D backbone, with pre-trained weights provided by FCOS3D [59], to extract image features. The feature maps from stage 1, 2, and 3 of the backbone are then fed into FPN [55], resulting in three levels of multi-scale image features. The network architecture consists of four levels ($L = 4$), with no skip connection applied to the highest level. Our framework is adaptable to any view transformation approach. In this paper, we choose the view transformation method proposed in InverseMatrixVT3D [14] to aggregate visual features. It is worth mentioning that when the framework does not merge lidar and radar information, it is the same as the InverseMatrixVT3D algorithm. Thus, OccFusion (C) has the same performance as InverseMatrixVT3D. To extract 3D feature volumes, the VoxelNet [32] is used as the framework’s 3D backbone, which processes the lidar dense 3D point cloud and the sparse 3D point cloud from surround-view radars. For optimization, the AdamW optimizer with an initial learning rate of $5e-5$ and weight decay of 0.01 is employed. The learning rate is decayed using a multi-step scheduler. During the training phase, the framework is trained using focal loss [60], Lovasz-softmax loss [61], and scene-class affinity loss [1]. To account for the importance of high-resolution 3D volumes over lower-resolution ones, a decayed loss weight $w = \frac{1}{2^l}$ is used for supervision at the l -th level. The model is trained on eight A10 GPUs, each with 24GB of memory, for two days to perform 3D semantic occupancy prediction task.

B. Dataset

We conducted our experiments on the nuScenes dataset. The ground truth labels for 3D semantic occupancy prediction were obtained from SurroundOcc’s work [7], and Occ3D [6]. The SurroundOcc’s label spans a range of -50 m to 50 m for the X and Y directions and -5 m to 3 m for the Z direction. This range is suitable for conducting our model’s ablation study on the perception range factor. On the other hand, the Occ3D provide a ground truth label for a relatively

minor perceptual range, which spans a range of -40 m to 40 m for the X and Y directions and -1 m to 5.4 m for the Z direction. Furthermore, since it was designed for purely vision-centric algorithms, a visibility mask is provided for each voxel grid, and evaluation only considers visible voxels. As the test set labels were unavailable, we trained our model on the training set and evaluated its performance on the validation set. Additionally, we chose particular frames from the nuScenes validation set, using ground truth labels from SurroundOcc’s work to establish subsets corresponding to rainy and night scenarios. The distribution of classes in the validation set, rainy scenario subset, and night scenario subset is shown in Figure 4. The class with a sample number equal to zero is not listed in each set.

C. Performance Evaluate Metrics

To evaluate the performance of different state-of-the-art (SOTA) algorithms and compare them with our approach in the task of 3D semantic occupancy prediction, we employ the intersection over union (IoU) to evaluate each semantic class. Additionally, we use the mean IoU across all semantic classes (mIoU) as a comprehensive evaluation metric:

$$IoU = \frac{TP}{TP + FP + FN} \quad (2)$$

and

$$mIoU = \frac{1}{Cls} \sum_{i=1}^{Cls} \frac{TP_i}{TP_i + FP_i + FN_i} \quad (3)$$

where TP , FP , and FN represent the counts of true positives, false positives, and false negatives in our predictions, respectively, while Cls denotes the total class number.

D. Model Performance Analysis

We assess different sensor fusion strategies using our proposed framework on the nuScenes validation set, and present the final benchmark results in Table I and Table II. In Table I, in comparison to purely vision-centric approaches, the inclusion of sparse 3D point cloud information from the surround-view radars leads to a noteworthy around 2% improvement in performance. Moreover, adding dense 3D point cloud information from the lidar further enhances the performance to approximately 27% mIoU. These experimental results confirm the efficacy of utilizing multi-sensor fusion to substantially improve the performance of the 3D semantic occupancy prediction task. However, in Table II, we observed a non-trivial performance degradation caused by merging radar information. This may attribute to the nature of radar, which is good at measuring objects that are far away, but the perception range in Occ3D’s label and the visibility mask limit its strength. In addition, radar readings are usually noisy, affecting the model’s judgment at close range.

E. Challenging Scenarios Performance Analysis

To gain deeper insights into sensor fusion properties and effectiveness, we assess various sensor fusion strategies in challenging nighttime and rainy scenarios. The performance

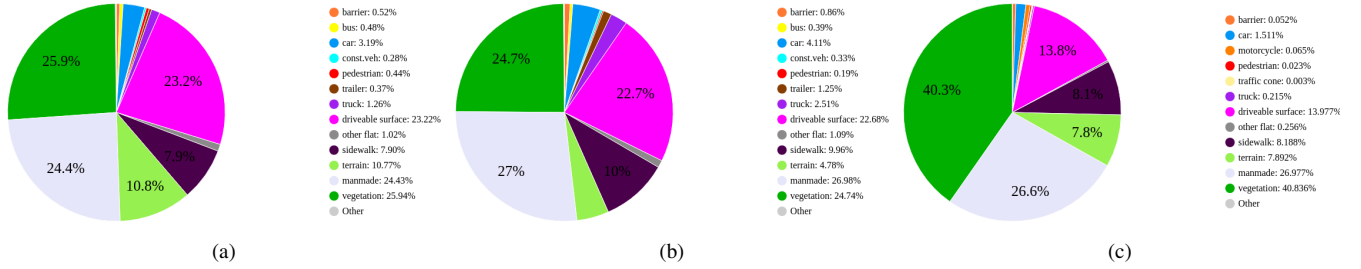


Fig. 4: Class distribution for three validation sets. (a) whole validation set class distribution, (b) rainy scenario subset class distribution, and (c) night scenario subset class distribution.

Method	Backbone	Input Modality	mIoU	barrier	bicycle	bus	car	const. veh.	motorcycle	pedestrian	traffic cone	trailer	truck	drive. surf.	other flat	sidewalk	terrain	manmade	vegetation
MonoScene [1]	R101-DCN	C	7.31	4.03	0.35	8.00	8.04	2.90	0.28	1.16	0.67	4.01	4.35	27.72	5.20	15.13	11.29	9.03	14.86
Atlas [62]	R101-DCN	C	15.00	10.64	5.68	19.66	24.94	8.90	8.84	6.47	3.28	10.42	16.21	34.86	15.46	21.89	20.95	11.21	20.54
BEVFormer [3]	R101-DCN	C	16.75	14.22	6.58	23.46	28.28	8.66	10.77	6.64	4.05	11.20	17.78	37.28	18.00	22.88	22.17	13.80	22.21
TPVFormer [5]	R101-DCN	C	17.10	15.96	5.31	23.86	27.32	9.79	8.74	7.09	5.20	10.97	19.22	38.87	21.25	24.26	23.15	11.73	20.81
C-CONet [63]	R101	C	18.40	18.60	10.00	26.40	27.40	8.60	15.70	13.30	9.70	10.90	20.20	33.00	20.70	21.40	21.80	14.70	21.30
InverseMatrixVT3D [14]	R101-DCN	C	18.88	18.39	12.46	26.30	29.11	11.00	15.74	14.78	11.38	13.31	21.61	36.30	19.97	21.26	20.43	11.49	18.47
RenderOcc [9]	R101	C	19.00	19.70	11.20	28.10	28.20	9.80	14.70	11.80	11.90	13.10	20.10	33.20	21.30	22.60	22.30	15.30	20.90
SurroundOcc [7]	R101-DCN	C	20.30	20.59	11.68	28.06	30.86	10.70	15.14	14.09	12.06	14.38	22.26	37.29	23.70	24.49	22.77	14.89	21.86
LMSCNet [64]	-	L	14.90	13.10	4.50	14.70	22.10	12.60	4.20	7.20	7.10	12.20	11.50	26.30	14.30	21.10	15.20	18.50	34.20
L-CONet [63]	-	L	17.70	19.20	4.00	15.10	26.90	6.20	3.80	6.80	6.00	14.10	13.10	39.70	19.10	24.00	23.90	25.10	35.70
M-CONet [63]	-	C+L	24.70	24.80	13.00	31.60	34.80	14.60	18.00	20.00	14.70	20.00	26.60	39.20	22.80	26.10	26.00	26.00	37.10
OccFusion	R101+VoxelNet	C+R	20.73	20.46	13.98	27.99	31.52	13.68	18.45	15.79	13.05	13.94	23.84	37.85	19.60	22.41	21.20	16.16	21.81
OccFusion	R101+VoxelNet	C+L	26.87	26.67	18.38	32.97	35.81	19.39	27.17	24.48	17.77	21.46	29.67	39.01	21.94	24.90	26.76	28.53	40.03
OccFusion	R101+VoxelNet	C+L+R	27.30	27.09	19.56	33.68	36.23	21.66	24.84	25.29	16.33	21.81	30.01	39.53	19.94	24.94	26.45	28.93	40.41

TABLE I: **3D semantic occupancy prediction results on nuScenes validation set.** All methods are trained with dense occupancy labels from [7]. Notion of modality: Camera (C), Lidar (L), Radar (R).

Method	Backbone	Input Modality	mIoU	others	barrier	bicycle	bus	car	const. veh.	motorcycle	pedestrian	traffic cone	trailer	truck	drive. surf.	other flat	sidewalk	terrain	manmade	vegetation
MonoScene [1]	EfficientNetB7	C	6.06	1.75	7.23	4.26	4.93	9.38	5.67	3.98	3.01	5.90	4.45	7.17	14.91	6.32	7.92	7.43	1.01	7.65
BEVDet [2]	ResNet101	C	11.73	2.09	15.29	0.0	4.18	12.97	1.35	0.0	0.43	0.13	6.59	6.66	52.72	19.04	26.45	21.78	14.51	15.26
BEVFormer [3]	ResNet101	C	23.67	5.03	38.79	9.98	34.41	41.09	13.24	16.50	18.15	17.83	18.66	27.70	48.95	27.73	29.08	25.38	15.41	14.46
BEVStereo [4]	ResNet101	C	24.51	5.73	38.41	7.88	38.70	41.20	17.56	17.33	14.69	10.31	16.84	29.62	54.08	28.92	32.68	26.54	18.74	17.49
TPVFormer [5]	ResNet101	C	28.34	6.67	39.20	14.24	41.54	46.98	19.21	22.64	17.87	14.54	30.20	35.51	56.18	33.65	35.69	31.61	19.97	16.12
OccFormer [20]	ResNet101	C	21.93	5.94	30.29	12.32	34.40	39.17	14.44	16.45	17.22	9.27	13.90	26.36	50.99	30.96	34.66	22.73	6.76	6.97
CTF-Occ [6]	ResNet101	C	28.53	8.09	39.33	20.56	38.29	42.24	16.93	24.52	22.72	21.05	22.98	31.11	53.33	33.84	37.98	33.23	20.79	18.00
RenderOcc [9]	ResNet101	C	26.11	4.84	31.72	10.72	27.67	26.45	13.87	18.20	17.67	17.84	21.19	23.25	63.20	36.42	46.21	44.26	19.58	20.72
BEVDet4D [10*]	Swin-B	C	42.02	12.15	49.63	25.10	52.02	54.46	27.87	27.99	28.94	27.23	36.43	42.22	82.31	43.29	54.46	57.90	48.61	43.55
PanoOcc [11]*	ResNet101	C	42.13	11.67	50.48	29.64	49.44	55.52	23.29	33.26	30.55	30.99	34.43	42.57	83.31	44.23	54.40	56.04	45.94	40.40
FB-Occ [12]*	ResNet101	C	43.41	12.10	50.23	32.31	48.55	52.89	31.20	31.25	30.78	32.33	37.06	40.22	83.34	49.27	57.13	59.88	47.67	41.76
OctreeOcc [13*]	ResNet101	C	44.02	11.96	51.70	29.93	53.52	56.77	30.83	33.17	30.65	29.99	37.76	43.87	83.17	44.52	55.45	58.86	49.52	46.33
OccFusion*	R101+VoxelNet	C+R	38.26	10.11	43.48	26.63	48.25	53.29	24.98	33.35	31.75	27.31	29.88	40.15	77.59	35.47	43.64	48.01	42.73	33.81
OccFusion*	R101+VoxelNet	C+L	46.79	11.65	47.81	32.07	57.27	57.51	31.80	40.11	47.35	33.74	45.81	50.35	78.79	37.17	44.36	53.36	63.18	63.20
OccFusion*	R101+VoxelNet	C+L+R	46.67	12.37	50.33	31.53	57.62	58.81	33.97	41.00	47.18	29.67	42.03	48.04	78.39	35.68	47.26	52.74	63.46	63.30

TABLE II: **3D semantic occupancy prediction results on Occ3D benchmark.** All methods are trained with dense occupancy labels from [6]. Notion of modality: Camera (C), Lidar (L), Radar (R). "*" denotes training with the camera mask.

of the models in these scenarios is presented in Table III and Table IV.

In the rainy scenario, despite the radar sensor being the most resilient to adverse weather conditions, integrating surround-view camera and radar information only leads to a marginal performance improvement of 0.2%. This outcome can be attributed to the nature of the 3D occupancy prediction task, which necessitates dense features. However, the sparse 3D point clouds provided by surround-view radars limit their contribution in rainy scenarios, thus resulting in a negligible impact. In comparison, despite the reflection issue it faces in rainy scenarios, the lidar sensor can still make a substantial contribution to the model's overall performance owing to its dense 3D point cloud. Another reason could be attributed to the absence of severe rainy conditions in the nuScenes dataset. The dataset primarily includes light to moderate rain scenarios,

wherein the lidar data maintains a consistently high quality. By integrating the information from all three sensors, our model achieves the best performance.

In nighttime scenarios, it is undeniable that purely vision-centric approaches perform poorly due to the sensitivity of surround-view cameras to varying illumination conditions. We found that integrating information from surround-view radars notably augmented the model's performance, leading to an approximate 1.2% enhancement. Furthermore, the inclusion of radar data significantly improves the capability to predict dynamic objects. Particularly, a performance boost of around 4% is observed for the car class. Likewise, we note performance gains of approximately 0.7% for bicycles and 3% for motorcycles as small dynamic objects. This progress is linked to the velocity measurement function of surround-view radars and demonstrates the effective integration of these

features with camera attributes within our framework. What’s more, the inclusion of lidar information yielded an additional performance gain of 4.7%.

F. Perception Range Impact On Model Performance

Multi-sensor fusion not only improves the final model’s robustness to different illumination and weather conditions but also extends the model’s perception range. We take the vehicle’s centre as the origin and R as the radius. By adjusting the length of R , we study the characteristics of different sensor fusion strategies under different perception ranges in different scenarios. We evaluate each model and different sensor fusion strategies at $R = [20m, 25m, 30m, 35m, 40m, 45m, 50m]$.

The performance variation trend of each model concerning R on the nuScenes validation set is depicted in Figure 5a. Our model achieves significantly improved performance by integrating radar and lidar data, particularly at longer ranges.

In the rainy scenario, the performance variation trend, depicted in Figure 5b, reveals the limited impact of radar information. Specifically, the variation trend of OccFusion(C+L) only slightly deviates from that of OccFusion(C+L+R) when the radius exceeds 30m. However, the performance trend of OccFusion(C) displays a notable discrepancy compared to OccFusion(C+R), and this difference becomes more pronounced as the perception range expands. This observation underscores the significant positive influence of radar information in enhancing the perception range and overall performance of vision-centric algorithms.

In the nighttime scenario, the variation trend of performance is shown in Figure 5c. It demonstrates that adding radar information significantly enhances the lidar’s ability to perceive objects at extended distances. Notably, the performance discrepancy between OccFusion (C+L+R) and OccFusion (C+L) increased as the perception range increased. This phenomenon can be attributed to radar sensors having the longest detection range. Additionally, despite radar features being sparse, their information can spread to nearby features from other modalities, thereby enhancing the information of the final merged feature.

G. Framework Qualitative Analysis

We conducted qualitative analysis by generating visualizations of recent state-of-the-art (SOTA) algorithms and comparing them with the prediction results from our framework with different sensor fusion strategies. The overall visualization result is demonstrated in Figure 6. In Figure 6 upper, we present the prediction results for the daytime scenario; in the middle, we show the prediction results for the rainy scenario; and at the bottom, we present the prediction results for the nighttime scenario. The main discrepancy of each prediction result under each scenario has been highlighted by a red rectangle.

In the daytime scenario, as shown in Figure 6 upper, algorithms that rely solely on surround-view cameras are unable to accurately predict pedestrians at remote distances, either failing to identify them or misestimating their numbers. This issue has been partially resolved by integrating radar

information with the camera, which means the radar data helps the model extend its perception range. Furthermore, the addition of lidar information has further enhanced the framework’s ability to model the 3D world, particularly in capturing the geometry and contour of static objects.

In the rainy scenario, as shown in Figure 6 middle, vision-centric algorithms have trouble predicting remote range overlay objects. By merging radar information with cameras, this issue has been mitigated a lot, but models still have trouble predicting the manmade buildings that hang in the sky. This issue is well solved by adding lidar data into the model. This visualization result reveals that three-sensor fusion extends the model perception range and enhances the model’s 3D world structure detail-capturing capability.

In the nighttime scenario, the surround-view cameras are susceptible to illumination changes and perform poorly in dim environments. As a result, it is not surprising that purely vision-centric algorithms yield terrible prediction results in such scenarios, as shown in Figure 6 bottom. Surprisingly, we found that even by adding only radar data, which provides a sparse 3D point cloud, the model significantly improves in predicting static objects such as vegetation and manmade structures. Furthermore, when lidar data is merged, the model’s prediction results improve significantly. It is worth noting that even after merging lidar data, the OccFusion (C+L+R) model fails to classify the nearby sidewalk. This phenomenon can be attributed to the fact that lidar sensors do not provide rich semantic information, and in this particular scenario, the camera’s semantic information is also significantly degraded.

H. Framework Training Convergence Speed Study

During the training phase, we observed that different sensor fusion strategies not only influence the framework’s ultimate performance but also have a notable impact on its overall training duration. As illustrated in Figure 7, OccFusion (C), a vision-centric method, required 13 training epochs to reach optimal performance. In contrast, OccFusion (C+R), integrating radar information with cameras, reduced the total training epochs to 9 and achieved approximately a 2% performance enhancement. Combining Lidar information with cameras further reduced the training epochs to 6, resulting in a performance improvement of 6%. This occurrence highlights the benefits of sensor fusion, which not only enhances the final framework performance but also accelerates its convergence speed during training.

I. Framework Efficiency Study

We assess the effectiveness of each sensor fusion strategy implemented in our framework and compare them with other state-of-the-art (SOTA) algorithms. Detailed information on the efficiency of the framework is provided in Table V. By incorporating more sensor information, our framework becomes more complex and necessitates a greater number of trainable parameters. Consequently, this leads to increased utilization of GPU memory and higher latency during inference.

Method	Backbone	Input Modality	mIoU	barrier	bicycle	bus	car	const. veh.	motorcycle	pedestrian	traffic cone	trailer	truck	drive. surf.	other flat	sidewalk	terrain	manmade	vegetation
				●	●	●	●	●	●	●	●	●	●	●	●	●	●	●	●
InverseMatrixVT3D [14]	R101-DCN	C	18.99	18.55	14.29	22.28	30.02	10.19	15.20	10.03	9.71	13.28	20.98	37.18	23.47	27.74	17.46	10.36	23.13
SurroundOcc [7]	R101-DCN	C	19.85	21.40	12.75	25.49	31.31	11.39	12.65	8.94	9.48	14.51	21.52	35.34	25.32	29.89	18.37	14.44	24.78
OccFusion	R101+VoxelNet	C+R	20.78	20.14	16.33	26.37	32.39	11.56	17.08	11.14	10.54	13.61	22.42	37.50	22.79	29.50	17.58	17.06	26.49
OccFusion	R101+VoxelNet	C+L	26.55	24.95	19.11	34.23	36.07	17.01	21.07	18.87	17.46	21.81	28.73	37.82	24.39	30.80	20.37	28.95	43.12
OccFusion	R101+VoxelNet	C+L+R	26.72	25.30	18.71	33.58	36.28	17.76	22.44	20.80	15.89	22.63	28.75	39.28	22.72	30.78	20.15	28.99	43.37

TABLE III: **3D semantic occupancy prediction results on nuScenes validation rainy scenario subset.** All methods are trained with dense occupancy labels from [7]. Notion of modality: Camera (C), Lidar (L), Radar (R).

Method	Backbone	Input Modality	mIoU	barrier	bicycle	bus	car	const. veh.	motorcycle	pedestrian	traffic cone	trailer	truck	drive. surf.	other flat	sidewalk	terrain	manmade	vegetation
				●	●	●	●	●	●	●	●	●	●	●	●	●	●	●	●
InverseMatrixVT3D [14]	R101-DCN	C	9.99	10.40	12.03	0.00	29.94	0.00	9.92	4.88	0.91	0.00	17.79	29.10	2.37	10.80	9.40	8.68	13.57
SurroundOcc [7]	R101-DCN	C	10.80	10.55	14.60	0.00	31.05	0.00	8.26	5.37	0.58	0.00	18.75	30.72	2.74	12.39	11.53	10.52	15.77
OccFusion	R101+VoxelNet	C+R	11.13	10.78	12.77	0.00	33.50	0.00	12.72	4.91	0.61	0.00	19.97	29.51	0.94	12.15	10.72	11.81	17.72
OccFusion	R101+VoxelNet	C+L	15.26	12.74	13.52	0.00	35.85	0.00	15.33	13.19	0.83	0.00	23.78	32.49	0.92	14.24	20.54	23.57	37.10
OccFusion	R101+VoxelNet	C+L+R	15.82	13.27	13.53	0.00	36.41	0.00	19.71	12.16	2.04	0.00	25.90	32.44	0.80	14.30	21.06	24.49	37.00

TABLE IV: **3D semantic occupancy prediction results on nuScenes validation night scenario subset.** All methods are trained with dense occupancy labels from [7]. Notion of modality: Camera (C), Lidar (L), Radar (R).

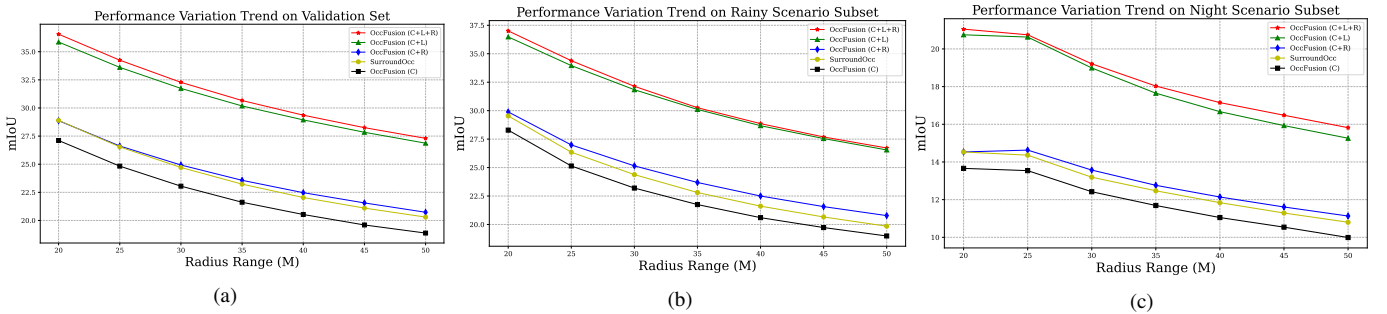


Fig. 5: Performance variation trend. (a) performance variation trend on whole nuScenes validation set, (b) performance variation trend on nuScenes validation rainy scenario subset, and (c) performance variation trend on nuScenes validation night scenario subset. **Better viewed when zoomed in.**

Method	Latency (ms) (↓)	Memory (GB) (↓)	Params
SurroundOcc [7]	472	5.98	180.51M
InverseMatrixVT3D [14]	447	4.41	67.18M
OccFusion(C+R)	588	5.56	92.71M
OccFusion(C+L)	591	5.56	92.71M
OccFusion(C+L+R)	601	5.78	114.97M

TABLE V: Model efficiency comparison of different methods. The experiments are performed on a single A10 using six multi-camera images, lidar, and radar data. For input image resolution, all methods adopt 1600×900 . ↓:the lower, the better.

J. Framework Ablation Study

1) *Ablation on multi-scale mechanism:* We investigated the influence of multi-level supervision and a multi-scale coarse-to-fine feature refinement structure on the overall performance. The ablation study result is shown in Table VI. The importance of the multi-scale mechanism in improving the performance of the final model is evident. The use of a multi-level supervision approach allows for the deeper levels to capture more general semantic information. Additionally, the multi-scale cores-to-fine refinement structure facilitates the passing of semantic information from deeper to shallower levels, thereby refining

Multi.Stru	Multi.Sup	Params	mIoU↑
✓	✓	114.97M	23.00%
✓	✗	114.97M	17.79%
✗	✗	54.99M	19.47%

TABLE VI: Ablation study results on the multi-scale mechanism used in the framework. Multi.Stru: multi-scale coarse-to-fine refinement structure, Multi.Sup: multi-level supervision mechanism. ↑:the higher, the better.

the highest-level feature, which is rich in spatial information. Another key finding from the ablation study is the strong correlation between the multi-scale coarse-to-fine structure and the multi-level supervision mechanism. This structure necessitates supervision signals at each scale to enable the framework to capture relevant semantic information and communicate it to higher levels. In the absence of such supervision signals, this design aspect can impede model convergence and result in suboptimal final performance.

2) *Ablation on Dynamic Fusion 3D/2D:* This study examines the impact of various sub-modules in dynamic fusion 3D/2D on the performance of the final model. Upon removing the BEV feature, thereby disabling the global-local attention

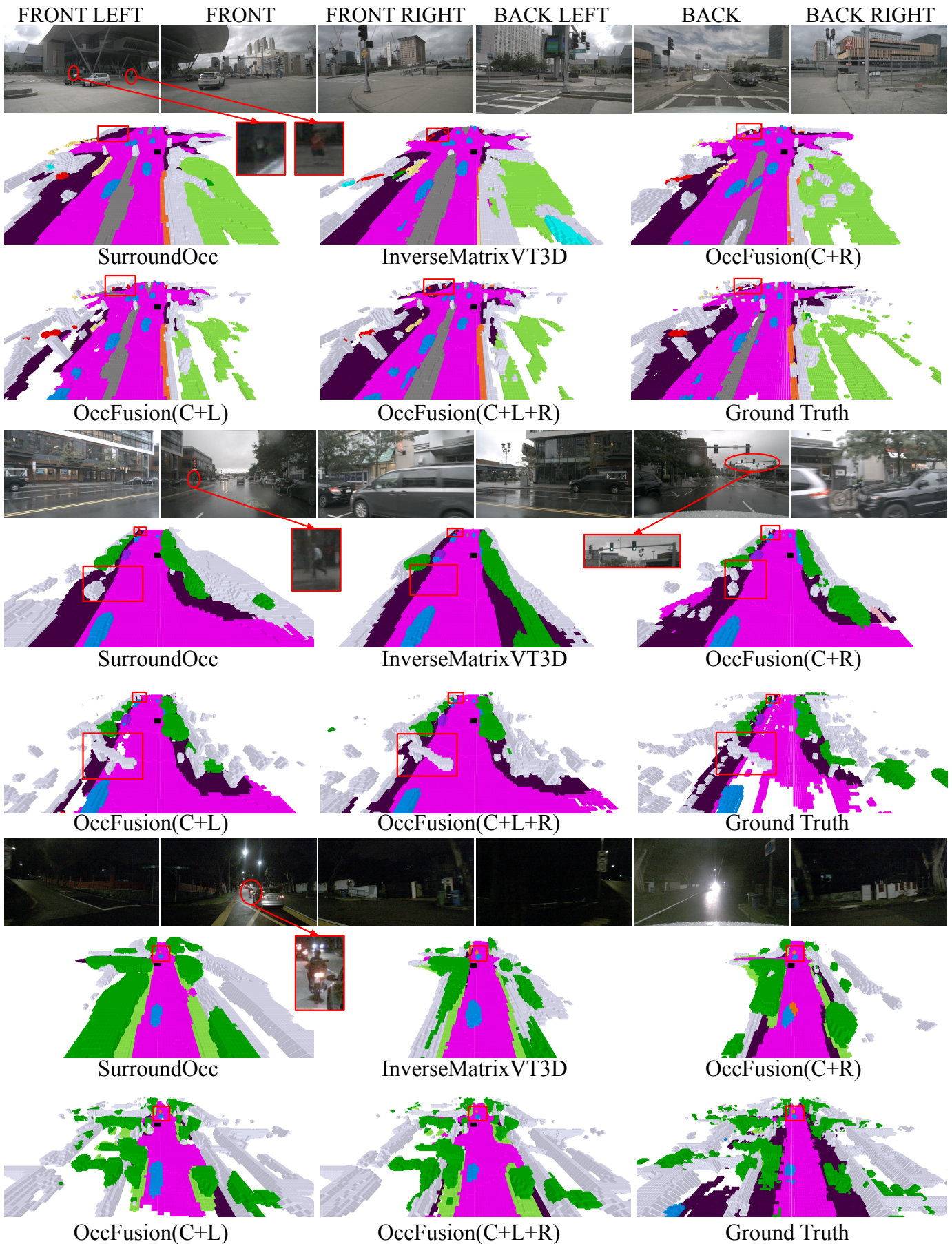


Fig. 6: Qualitative results for daytime, rainy, and nighttime scenarios displayed in the upper, middle, and bottom sections, respectively. **Better viewed when zoomed in.** Notion of modality: Camera (C), Lidar (L), Radar (R).

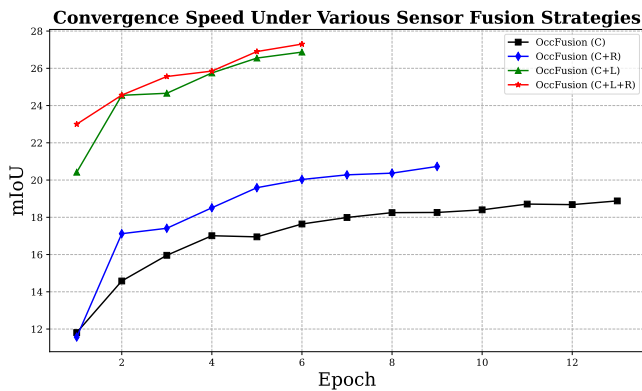


Fig. 7: The convergence speed of the framework during the training phase under various sensor fusion strategies. Notion of modality: Camera (C), Lidar (L), Radar (R).

BEV	SENet2D	SENet3D	mIoU↑
✓	✓	✓	23.00%
✗	✗	✓	16.37%
✓	✓	✗	19.01%
✓	✗	✓	19.94%

TABLE VII: Ablation study results on the dynamic fusion 3D/2D module used in the framework. BEV: merged BEV feature, SENet2D: senet block 2D part used to fuse multi-modality BEV features, SENet3D: senet block 3D part used to fuse multi-modality 3D feature volumes. ↑: the higher the better.

fusion module, the model’s performance decreased by approximately 6.7%. This observation suggests that the BEV feature plays a crucial role as an excitation signal, facilitating interaction with the 3D feature volume to enable rapid convergence and capture of 3D geometric information. By removing the SENet3D/2D block in the dynamic fusion module, our model achieves feature fusion solely through feature channel concatenation, devoid of any feature amplification operation. As crucial features remain unamplified, our model experiences a significant performance drop.

V. CONCLUSION

In this study, we present OccFusion, a novel framework that integrates surround-view cameras, radars, and lidar for the prediction of 3D semantic occupancy. Our framework employs dynamic fusion 3D/2D modules to consolidate features from diverse modalities, generating a comprehensive 3D volume. The fusion strategies examined in this research encompass Camera+Radar, Camera+Lidar, and Camera+Lidar+Radar combinations. Through a comprehensive evaluation on the nuScenes validation set, as well as subsets focusing on night and rainy scenarios, we thoroughly analyze the overall performance of each fusion strategy implemented by OccFusion. Additionally, we investigate the impact of perception range on the performance trends of each sensor fusion strategy across different perception ranges. Our experiments exhibit the

effectiveness of the OccFusion framework while preserving the distinct strengths of each sensor.

REFERENCES

- [1] A.-Q. Cao and R. de Charette, “Monoscene: Monocular 3d semantic scene completion,” in *Proceedings of the IEEE/CVF Conference on Computer Vision and Pattern Recognition*, 2022, pp. 3991–4001.
- [2] J. Huang, G. Huang, Z. Zhu, Y. Ye, and D. Du, “Bvdet: High-performance multi-camera 3d object detection in bird-eye-view,” *arXiv preprint arXiv:2112.11790*, 2021.
- [3] Z. Li, W. Wang, H. Li, E. Xie, C. Sima, T. Lu, Y. Qiao, and J. Dai, “Bevformer: Learning bird’s-eye-view representation from multi-camera images via spatiotemporal transformers,” in *European conference on computer vision*. Springer, 2022, pp. 1–18.
- [4] Y. Li, H. Bao, Z. Ge, J. Yang, J. Sun, and Z. Li, “Bevstereo: Enhancing depth estimation in multi-view 3d object detection with temporal stereo,” in *Proceedings of the AAAI Conference on Artificial Intelligence*, vol. 37, no. 2, 2023, pp. 1486–1494.
- [5] Y. Huang, W. Zheng, Y. Zhang, J. Zhou, and J. Lu, “Tri-perspective view for vision-based 3d semantic occupancy prediction,” in *Proceedings of the IEEE/CVF Conference on Computer Vision and Pattern Recognition*, 2023, pp. 9223–9232.
- [6] X. Tian, T. Jiang, L. Yun, Y. Wang, Y. Wang, and H. Zhao, “Occ3d: A large-scale 3d occupancy prediction benchmark for autonomous driving,” *arXiv preprint arXiv:2304.14365*, 2023.
- [7] Y. Wei, L. Zhao, W. Zheng, Z. Zhu, J. Zhou, and J. Lu, “Surroundocc: Multi-camera 3d occupancy prediction for autonomous driving,” in *Proceedings of the IEEE/CVF International Conference on Computer Vision*, 2023, pp. 21 729–21 740.
- [8] H. Zhang, X. Yan, D. Bai, J. Gao, P. Wang, B. Liu, S. Cui, and Z. Li, “Radocc: Learning cross-modality occupancy knowledge through rendering assisted distillation,” *arXiv preprint arXiv:2312.11829*, 2023.
- [9] M. Pan, J. Liu, R. Zhang, P. Huang, X. Li, L. Liu, and S. Zhang, “Renderocc: Vision-centric 3d occupancy prediction with 2d rendering supervision,” *arXiv preprint arXiv:2309.09502*, 2023.
- [10] J. Huang and G. Huang, “Bvdet4d: Exploit temporal cues in multi-camera 3d object detection,” *arXiv preprint arXiv:2203.17054*, 2022.
- [11] Y. Wang, Y. Chen, X. Liao, L. Fan, and Z. Zhang, “Panoocc: Unified occupancy representation for camera-based 3d panoptic segmentation,” *arXiv preprint arXiv:2306.10013*, 2023.
- [12] Z. Li, Z. Yu, D. Austin, M. Fang, S. Lan, J. Kautz, and J. M. Alvarez, “Fb-occ: 3d occupancy prediction based on forward-backward view transformation,” *arXiv preprint arXiv:2307.01492*, 2023.
- [13] Y. Lu, X. Zhu, T. Wang, and Y. Ma, “Octreeocc: Efficient and multi-granularity occupancy prediction using octree queries,” *arXiv preprint arXiv:2312.03774*, 2023.
- [14] Z. Ming, J. S. Berrio, M. Shan, and S. Worrall, “Inversematrixvt3d: An efficient projection matrix-based approach for 3d occupancy prediction,” *arXiv preprint arXiv:2401.12422*, 2024.
- [15] H. Caesar, V. Bankiti, A. H. Lang, S. Vora, V. E. Liong, Q. Xu, A. Krishnan, Y. Pan, G. Baldan, and O. Beijbom, “nusenes: A multimodal dataset for autonomous driving,” in *Proceedings of the IEEE/CVF conference on computer vision and pattern recognition*, 2020, pp. 11 621–11 631.
- [16] J. Philion and S. Fidler, “Lift, splat, shoot: Encoding images from arbitrary camera rigs by implicitly unprojecting to 3d,” in *Computer Vision—ECCV 2020: 16th European Conference, Glasgow, UK, August 23–28, 2020, Proceedings, Part XIV 16*. Springer, 2020, pp. 194–210.
- [17] Y. Li, Z. Ge, G. Yu, J. Yang, Z. Wang, Y. Shi, J. Sun, and Z. Li, “Bevdepth: Acquisition of reliable depth for multi-view 3d object detection,” in *Proceedings of the AAAI Conference on Artificial Intelligence*, vol. 37, no. 2, 2023, pp. 1477–1485.
- [18] C. Yang, Y. Chen, H. Tian, C. Tao, X. Zhu, Z. Zhang, G. Huang, H. Li, Y. Qiao, L. Lu *et al.*, “Bevformer v2: Adapting modern image backbones to bird’s-eye-view recognition via perspective supervision,” in *Proceedings of the IEEE/CVF Conference on Computer Vision and Pattern Recognition*, 2023, pp. 17 830–17 839.
- [19] Y. Zhang, Z. Zhu, W. Zheng, J. Huang, G. Huang, J. Zhou, and J. Lu, “Beverse: Unified perception and prediction in birds-eye-view for vision-centric autonomous driving,” *arXiv preprint arXiv:2205.09743*, 2022.
- [20] Y. Zhang, Z. Zhu, and D. Du, “Occformer: Dual-path transformer for vision-based 3d semantic occupancy prediction,” *arXiv preprint arXiv:2304.05316*, 2023.

- [21] S. F. Bhat, I. Alhashim, and P. Wonka, "Adabins: Depth estimation using adaptive bins," in *Proceedings of the IEEE/CVF Conference on Computer Vision and Pattern Recognition*, 2021, pp. 4009–4018.
- [22] R. Cheng, R. Razani, E. Taghavi, E. Li, and B. Liu, "2-s3net: Attentive feature fusion with adaptive feature selection for sparse semantic segmentation network," in *Proceedings of the IEEE/CVF conference on computer vision and pattern recognition*, 2021, pp. 12 547–12 556.
- [23] V. E. Liong, T. N. T. Nguyen, S. Widjaja, D. Sharma, and Z. J. Chong, "Amvnet: Assertion-based multi-view fusion network for lidar semantic segmentation," *arXiv preprint arXiv:2012.04934*, 2020.
- [24] Y. Zhang, Z. Zhou, P. David, X. Yue, Z. Xi, B. Gong, and H. Foroosh, "Polarnet: An improved grid representation for online lidar point clouds semantic segmentation," in *Proceedings of the IEEE/CVF Conference on Computer Vision and Pattern Recognition*, 2020, pp. 9601–9610.
- [25] Q. Chen, S. Vora, and O. Beijbom, "Polarstream: Streaming object detection and segmentation with polar pillars," *Advances in Neural Information Processing Systems*, vol. 34, pp. 26 871–26 883, 2021.
- [26] X. Yan, J. Gao, J. Li, R. Zhang, Z. Li, R. Huang, and S. Cui, "Sparse single sweep lidar point cloud segmentation via learning contextual shape priors from scene completion," in *Proceedings of the AAAI Conference on Artificial Intelligence*, vol. 35, no. 4, 2021, pp. 3101–3109.
- [27] S. Li, X. Chen, Y. Liu, D. Dai, C. Stachniss, and J. Gall, "Multi-scale interaction for real-time lidar data segmentation on an embedded platform," *IEEE Robotics and Automation Letters*, vol. 7, no. 2, pp. 738–745, 2021.
- [28] H. Tang, Z. Liu, S. Zhao, Y. Lin, J. Lin, H. Wang, and S. Han, "Searching efficient 3d architectures with sparse point-voxel convolution," in *European conference on computer vision*. Springer, 2020, pp. 685–702.
- [29] H. Zhou, X. Zhu, X. Song, Y. Ma, Z. Wang, H. Li, and D. Lin, "Cylinder3d: An effective 3d framework for driving-scene lidar semantic segmentation," *arXiv preprint arXiv:2008.01550*, 2020.
- [30] M. Ye, R. Wan, S. Xu, T. Cao, and Q. Chen, "Drinet++: Efficient voxel-as-point point cloud segmentation," *arXiv preprint arXiv:2111.08318*, 2021.
- [31] D. Ye, Z. Zhou, W. Chen, Y. Xie, Y. Wang, P. Wang, and H. Foroosh, "Lidarmultinet: Towards a unified multi-task network for lidar perception," in *Proceedings of the AAAI Conference on Artificial Intelligence*, vol. 37, no. 3, 2023, pp. 3231–3240.
- [32] Y. Zhou and O. Tuzel, "Voxelnet: End-to-end learning for point cloud based 3d object detection," in *Proceedings of the IEEE conference on computer vision and pattern recognition*, 2018, pp. 4490–4499.
- [33] A. H. Lang, S. Vora, H. Caesar, L. Zhou, J. Yang, and O. Beijbom, "Pointpillars: Fast encoders for object detection from point clouds," in *Proceedings of the IEEE/CVF conference on computer vision and pattern recognition*, 2019, pp. 12 697–12 705.
- [34] T. Khurana, P. Hu, D. Held, and D. Ramanan, "Point cloud forecasting as a proxy for 4d occupancy forecasting," in *IEEE/CVF Conference on Computer Vision and Pattern Recognition (CVPR)*, 2023.
- [35] X. Liu, M. Gong, Q. Fang, H. Xie, Y. Li, H. Zhao, and C. Feng, "Lidar-based 4d occupancy completion and forecasting," *arXiv preprint arXiv:2310.11239*, 2023.
- [36] C. R. Qi, W. Liu, C. Wu, H. Su, and L. J. Guibas, "Frustum pointnets for 3d object detection from rgb-d data," in *Proceedings of the IEEE conference on computer vision and pattern recognition*, 2018, pp. 918–927.
- [37] Z. Yang, Y. Sun, S. Liu, X. Shen, and J. Jia, "Ipod: Intensive point-based object detector for point cloud," *arXiv preprint arXiv:1812.05276*, 2018.
- [38] X. Zhao, Z. Liu, R. Hu, and K. Huang, "3d object detection using scale invariant and feature reweighting networks," in *Proceedings of the AAAI Conference on Artificial Intelligence*, vol. 33, no. 01, 2019, pp. 9267–9274.
- [39] S. Vora, A. H. Lang, B. Helou, and O. Beijbom, "Pointpainting: Sequential fusion for 3d object detection," in *Proceedings of the IEEE/CVF conference on computer vision and pattern recognition*, 2020, pp. 4604–4612.
- [40] V. A. Sindagi, Y. Zhou, and O. Tuzel, "Mvx-net: Multimodal voxelnet for 3d object detection," in *2019 International Conference on Robotics and Automation (ICRA)*. IEEE, 2019, pp. 7276–7282.
- [41] M. Liang, B. Yang, S. Wang, and R. Urtasun, "Deep continuous fusion for multi-sensor 3d object detection," in *Proceedings of the European conference on computer vision (ECCV)*, 2018, pp. 641–656.
- [42] Z. Liu, H. Tang, A. Amini, X. Yang, H. Mao, D. L. Rus, and S. Han, "Bevfusion: Multi-task multi-sensor fusion with unified bird's-eye view representation," in *2023 IEEE International Conference on Robotics and Automation (ICRA)*. IEEE, 2023, pp. 2774–2781.
- [43] T. Liang, H. Xie, K. Yu, Z. Xia, Z. Lin, Y. Wang, T. Tang, B. Wang, and Z. Tang, "Befusion: A simple and robust lidar-camera fusion framework," *Advances in Neural Information Processing Systems*, vol. 35, pp. 10 421–10 434, 2022.
- [44] Y. Xie, C. Xu, M.-J. Rakotosaona, P. Rim, F. Tombari, K. Keutzer, M. Tomizuka, and W. Zhan, "Sparsefusion: Fusing multi-modal sparse representations for multi-sensor 3d object detection," *arXiv preprint arXiv:2304.14340*, 2023.
- [45] V. Guizilini, I. Vasiljevic, R. Ambrus, G. Shakhnarovich, and A. Gaidon, "Full surround monodepth from multiple cameras," *IEEE Robotics and Automation Letters*, vol. 7, no. 2, pp. 5397–5404, 2022.
- [46] Y. Li, J. Deng, Y. Zhang, J. Ji, H. Li, and Y. Zhang, "ezfusion: A close look at the integration of lidar, millimeter-wave radar, and camera for accurate 3d object detection and tracking," *IEEE Robotics and Automation Letters*, vol. 7, no. 4, pp. 11 182–11 189, 2022.
- [47] M. Bijelic, T. Gruber, F. Mannan, F. Kraus, W. Ritter, K. Dietmayer, and F. Heide, "Seeing through fog without seeing fog: Deep multi-modal sensor fusion in unseen adverse weather," in *Proceedings of the IEEE/CVF Conference on Computer Vision and Pattern Recognition*, 2020, pp. 11 682–11 692.
- [48] B. Major, D. Fontijne, A. Ansari, R. Teja Sukhvasi, R. Gowaikar, M. Hamilton, S. Lee, S. Grzechnik, and S. Subramanian, "Vehicle detection with automotive radar using deep learning on range-azimuth-doppler tensors," in *Proceedings of the IEEE/CVF International Conference on Computer Vision Workshops*, 2019, pp. 0–0.
- [49] R. Nabati and H. Qi, "Centerfusion: Center-based radar and camera fusion for 3d object detection," in *Proceedings of the IEEE/CVF Winter Conference on Applications of Computer Vision*, 2021, pp. 1527–1536.
- [50] R. Yadav, A. Vierling, and K. Berns, "Radar+ rgb fusion for robust object detection in autonomous vehicle," in *2020 IEEE International Conference on Image Processing (ICIP)*. IEEE, 2020, pp. 1986–1990.
- [51] R. Ravindran, M. J. Santora, and M. M. Jamali, "Camera, lidar, and radar sensor fusion based on bayesian neural network (clr-bnn)," *IEEE Sensors Journal*, vol. 22, no. 7, pp. 6964–6974, 2022.
- [52] X. Chen, T. Zhang, Y. Wang, Y. Wang, and H. Zhao, "Futr3d: A unified sensor fusion framework for 3d detection," in *Proceedings of the IEEE/CVF Conference on Computer Vision and Pattern Recognition*, 2023, pp. 172–181.
- [53] A. W. Harley, Z. Fang, J. Li, R. Ambrus, and K. Fragkiadaki, "Simplebev: What really matters for multi-sensor bev perception?" in *2023 IEEE International Conference on Robotics and Automation (ICRA)*. IEEE, 2023, pp. 2759–2765.
- [54] K. He, X. Zhang, S. Ren, and J. Sun, "Deep residual learning for image recognition," in *Proceedings of the IEEE conference on computer vision and pattern recognition*, 2016, pp. 770–778.
- [55] T.-Y. Lin, P. Dollár, R. Girshick, K. He, B. Hariharan, and S. Belongie, "Feature pyramid networks for object detection," in *Proceedings of the IEEE conference on computer vision and pattern recognition*, 2017, pp. 2117–2125.
- [56] J. Hu, L. Shen, and G. Sun, "Squeeze-and-excitation networks," in *Proceedings of the IEEE conference on computer vision and pattern recognition*, 2018, pp. 7132–7141.
- [57] K. He, X. Zhang, S. Ren, and J. Sun, "Deep residual learning for image recognition," in *Proceedings of the IEEE conference on computer vision and pattern recognition*, 2016, pp. 770–778.
- [58] J. Dai, H. Qi, Y. Xiong, Y. Li, G. Zhang, H. Hu, and Y. Wei, "Deformable convolutional networks," in *Proceedings of the IEEE international conference on computer vision*, 2017, pp. 764–773.
- [59] T. Wang, X. Zhu, J. Pang, and D. Lin, "Fcos3d: Fully convolutional one-stage monocular 3d object detection," in *Proceedings of the IEEE/CVF International Conference on Computer Vision*, 2021, pp. 913–922.
- [60] T.-Y. Lin, P. Goyal, R. Girshick, K. He, and P. Dollár, "Focal loss for dense object detection," in *Proceedings of the IEEE international conference on computer vision*, 2017, pp. 2980–2988.
- [61] M. Berman, A. R. Triki, and M. B. Blaschko, "The lovász-softmax loss: A tractable surrogate for the optimization of the intersection-over-union measure in neural networks," in *Proceedings of the IEEE conference on computer vision and pattern recognition*, 2018, pp. 4413–4421.
- [62] Z. Murez, T. Van As, J. Bartolozzi, A. Sinha, V. Badrinarayanan, and A. Rabinovich, "Atlas: End-to-end 3d scene reconstruction from posed images," in *Computer Vision—ECCV 2020: 16th European Conference, Glasgow, UK, August 23–28, 2020, Proceedings, Part VII 16*. Springer, 2020, pp. 414–431.
- [63] X. Wang, Z. Zhu, W. Xu, Y. Zhang, Y. Wei, X. Chi, Y. Ye, D. Du, J. Lu, and X. Wang, "Openoccupancy: A large scale benchmark for surrounding semantic occupancy perception," in *Proceedings of the*

IEEE/CVF International Conference on Computer Vision, 2023, pp. 17 850–17 859.

- [64] L. Roldão, R. de Charette, and A. Verroust-Blondet, “Lmscnet: Lightweight multiscale 3d semantic completion,” 2020.